**THE EUROPEAN
PHYSICAL JOURNAL D**

Calculations of multipole transitions in Sn II for kilonova analysis

A. I. Bondarev[1,2,a] (iD), J. H. Gillanders[3], C. Cheung[4], M. S. Safronova[4,5], and S. Fritzsche[1,2,6]

[1] GSI Helmholtzzentrum für Schwerionenforschung, Planckstr. 1, 64291 Darmstadt, Germany
[2] Helmholtz Institute Jena, Fröbelstieg 3, 07743 Jena, Germany
[3] Department of Physics, University of Rome "Tor Vergata", via della Ricerca Scientifica 1, 00133 Rome, Italy
[4] Department of Physics and Astronomy, University of Delaware, Newark, Delaware 19716, USA
[5] Joint Quantum Institute, National Institute of Standards and Technology and the University of Maryland, College Park, MD 20742, USA
[6] Institute for Theoretical Physics, Friedrich Schiller University, 07743 Jena, Germany

Abstract. We use the method that combines linearized coupled-cluster and configuration interaction approaches for calculating energy levels and multipole transition probabilities in singly ionized tin ions. We show that our calculated energies agree very well with the experimental data. We present probabilities of magnetic dipole and electric quadrupole transitions and use them for the analysis of the AT2017gfo kilonova emission spectra. This study demonstrates the importance and utility of accurate atomic data for forbidden transitions in the examination of future kilonova events.

1 Introduction

Forbidden transitions, namely the magnetic dipole (M1) and the electric quadrupole (E2), have been of interest in astronomy for a long time [1,2]. They are important in low-density plasma for the study of planetary nebulae, active galactic nuclei, and the interstellar medium [3].

Recent observations of the kilonova (KN) AT2017gfo [4,5], an astronomical transient associated with the gravitational wave signal from the binary neutron star merger GW170817 [6], provided much needed data for studying the origin of heavy elements in the universe [7,8]. The analysis of the AT2017gfo light curves strongly supports that the source of electromagnetic emission was the radioactive decay of elements synthesized by the rapid neutron capture process (r-process) in plasma ejected from the merger site during or after the collision [9]. However, in order to gain more insight into the composition of the ejecta, a spectroscopic line identification of particular elements is essential.

Certain features in the observed kilonova spectra were attempted to be attributed to absorption electric dipole (E1) lines of several ions: Cs I and Te I [5]; Sr II [10]; La III and Ce III [11]; and some others. Forbidden transitions are, in turn, relevant for exploring

features in the later phase spectra of AT2017gfo. In particular, Hotokezaka et al. [12] suggested that infrared emission at 4.5 μm in the nebular phase of the kilonova detected by the Spitzer Space Telescope [13] could originate from M1 transitions of W III, Os III, Rh III, Ce IV or Se III ions. They pointed out that the lack of accurate atomic data certainly complicates the modeling of the observed peculiar emission features.

The impact of magnetic dipole and electric quadrupole transitions on kilonova modeling was recently discussed by Gillanders et al. [14], who derived the limits on masses of produced platinum and gold in the AT2017gfo spectra. They also show how the inclusion of new atomic data of heavy elements can lead to the identification of elemental signatures through radiative transfer calculations.

Later, Gillanders et al. [15] concluded that it is most important to improve atomic data for tin, together with other elements belonging to the second r-process peak, such as ruthenium and tellurium. The typical ionization stages of elements related to the kilonova exploration depend on the ejecta temperature and the time after the merger. For observation times greater than one day, the synthesized elements are presumed to be present in stages from neutral to triply ionized [16].

Apart from kilonova modeling, singly ionized tin, which is a subject of the present investigation, is essential in astronomy to gain insight into nucleosynthesis governed by the slow neutron capture process (s-process) [17,18]. It is also promising for the diagnosis

of erosion of the vessel walls of future fusion power plants [19]. Therefore, the spectrum and transitions of this element were intensively studied both experimentally [20–23] and theoretically [24–27]. For a more detailed overview of publications prior to 2014, we refer to the work of Haris et al. [28], the main data source of the current NIST ASD for Sn II [29]. After that work, Heidarian et al. [30] reported measurements and multiconfiguration Dirac–Hartree–Fock (MCDHF) calculations of oscillator strengths of several transitions. Atalay et al. [31] used the same method and performed more elaborate calculations that also take into account core-valence correlations, for a larger number of energy levels and E1 transitions.

In the present work, we report calculations of low-lying energy levels and multipole (E1, M1, E2) transition probabilities in Sn II using the CI+all-order method that combines linearized coupled-cluster and configuration interaction approaches [32]. We use the atomic data to analyze the AT2017gfo spectra and show that forbidden transitions in Sn II could lead to detectable features in the kilonova emission spectra.

The paper is organized as follows. In Sect. 2, we briefly introduce the CI+all-order method and give details of the atomic computations. The results are presented and discussed in Sect. 3. In Sect. 4, we use these results to construct Sn II synthetic emission spectra and compare them with the observed AT2017gfo spectra. The conclusions are given in Sect. 5.

2 Theory

In our atomic computations, we use the method that combines configuration interaction (CI) with a linearized coupled-cluster approach (all order) [32]. In this method, the coupled-cluster approach is used to construct an effective Hamiltonian H_{eff} that includes core-core and core-valence correlations. The configuration interaction calculation is then done for valence electrons using the effective Hamiltonian rather than the usual bare Hamiltonian to incorporate core correlations. Briefly, the many-electron wave function is represented by a linear combination of Slater determinants,

$$\Psi = \sum_i c_i \Phi_i. \tag{1}$$

The pure CI Hamiltonian has a form

$$H_{\text{CI}} = E_{\text{core}} + \sum_{i>N_{\text{core}}} h_i^{\text{CI}} + \sum_{j>i>N_{\text{core}}} V_{ij}, \tag{2}$$

where E_{core} is the energy of the frozen core and N_{core} is the number of core electrons. The second term is a one-body operator that describes the kinetic energy of valence electrons and their interaction with the nucleus and core electrons. The last term is a two-body operator describing the electron–electron interaction. The Breit interaction is included in H_{CI} on the same footing as the Coulomb interaction. The core-valence correlation potential $\Sigma = \Sigma_1 + \Sigma_2$, consisting of the one-electron Σ_1 and two-electron Σ_2 parts, is obtained using the coupled-cluster method with single and double excitation [32]. It is added to the pure CI Hamiltonian to form the effective Hamiltonian for the CI+all-order calculation:

$$H_{\text{eff}} = H_{\text{CI}} + \Sigma. \tag{3}$$

The quantum electrodynamics (QED) corrections are also taken into account following [33,34].

We treat Sn II as a three-electron system with a $[1s^2 2s^2 2p^6 3s^2 3p^6 3d^{10} 4s^2 4p^6 4d^{10}]$ frozen core. Therefore, the three outer electrons were explicitly correlated using CI, while the contribution from 46 core electrons was taken into account by the coupled-cluster method and included via the effective Hamiltonian. We solve the Dirac–Hartree–Fock equations in the V^{N-3} potential, where N is the total number of electrons, to generate all core and 5-9s, 5-8p, 5-7d, and 4-6f valence orbitals. Other (virtual) orbitals were constructed by adding B-splines to the valence orbitals and diagonalizing the Dirac–Fock Hamiltonian. Employing the all-order method, we evaluated corrections to the one- and two-electron radial integrals that include valence orbitals. The CI space was constructed by making all possible single and double excitations from reference configurations to the 20$spdfg$ basis set. Several low-lying configurations were taken as reference ones; thus, the resulting configuration space also includes configurations with all three electrons excited compared to the ground state. We checked the convergence of the CI calculation by increasing the configuration space by allowing excitations to virtual states with larger principal quantum numbers and taking more reference configurations, verifying that the resulting changes in energy values were small.

Once the many-electron wave functions of individual states are computed, the reduced matrix elements of the multipole transition operators are calculated using the transition matrix formalism [35]. The random phase approximation corrections are included in the matrix element calculation. However, for E2 and, especially, M1 transitions, these corrections were found to be less important than for E1 transitions.

3 Results

In Table 1, we present the comparison of our results for low-energy levels of Sn II with the experimental values from the NIST ASD [29] and the most complete to date theoretical calculations of Atalay et al. [31].

We see that our results lie close to the experimental values with a maximum deviation of around 1.2% for the levels of the lowest even parity $5s5p^2$ configuration. For the levels of odd parity configurations, the differences with the experiment are much smaller. Furthermore, the differences for the lowest even levels have

Table 1 Comparison of the present CI+all-order energy levels (in cm^{-1}) in Sn II with the experimental values from the NIST ASD [29] and the theoretical results of Atalay et al. [31]

Level	NIST [29]	This work	ΔE^a	g factor	Atalay et al. [31]	ΔE^b
$5s^25p\,^2P^o_{1/2}$	0.00	0	0	0.67	0	0
$5s^25p\,^2P^o_{3/2}$	4251.494	4253	-2	1.33	4261	-10
$5s5p^2\,^4P_{1/2}$	46464.290	47035	-571	2.66	46370	94
$5s5p^2\,^4P_{3/2}$	48368.185	48961	-593	1.73	48243	125
$5s5p^2\,^4P_{5/2}$	50730.224	51323	-593	1.58	50626	104
$5s^26s\,^2S_{1/2}$	56886.363	56894	-8	2.00	56874	12
$5s5p^2\,^2D_{3/2}$	58844.181	59253	-409	0.81	58971	-127
$5s5p^2\,^2D_{5/2}$	59463.481	59943	-480	1.21	59558	-95
$5s^25d\,^2D_{3/2}$	71406.142	71516	-110	0.81	71746	-340
$5s^26p\,^2P^o_{1/2}$	71493.273	71460	33	0.67	71721	-228
$5s^25d\,^2D_{5/2}$	72048.260	72182	-134	1.20	72404	-356
$5s^26p\,^2P^o_{3/2}$	72377.448	72343	34	1.33	72582	-205
$5s5p^2\,^2S_{1/2}$	75954.3	76071	-117	1.34	76196	-242
$5s5p^2\,^2P_{1/2}$	80455.1	80555	-100	1.35	80735	-280
$5s5p^2\,^2P_{3/2}$	81718.3	81607	111	1.32	81714	4
$5s^27s\,^2S_{1/2}$	86280.318	86235	45	2.00	86309	-29
$5s^24f\,^2F^o_{7/2}$	89288.255	89213	75	1.14	89635	-347
$5s^24f\,^2F^o_{5/2}$	89294.055	89218	76	0.86	89639	-345
$5s^26d\,^2D_{3/2}$	90241.554	90213	29	0.80	90232	10
$5s^26d\,^2D_{5/2}$	90351.894	90371	-19	1.20	90344	8
$5s^27p\,^2P^o_{1/2}$	91903.945	91883	21	0.67	92031	-127
$5s^27p\,^2P^o_{3/2}$	92268.106	92259	9	1.33	92387	-119
$5s^28s\,^2S_{1/2}$	98402.412	98609	-207	2.00		

The differences between the theoretical and experimental values are also displayed. In addition, our calculated Landé g factors are shown

^{a} The difference between the present results and experimental energies from the NIST ASD [29]

^{b} The difference between the MCDHF results of Atalay et al. [31] and experimental energies from the NIST ASD [29]

the same sign. Thus, the accuracy of our wavelengths used in the calculation of M1 and E2 transitions is better than the accuracy for specific levels. The differences between our results and the experimental values are comparable to those between the MCDHF results of Ref. [31] and the experiment. The earlier theoretical estimations of energy levels, e.g., by Heidarian et al. [30], have markedly larger deviations from the experiment that grow with increasing excitation energy and are not shown here. In the table, one also finds the calculated values of Landé g factors. However, we should note that these values are very close to the results obtained using the formula

$$g_{\mathrm{nr}} = 1 + \frac{J(J+1) - L(L+1) + S(S+1)}{2J(J+1)} \qquad (4)$$

with parameters J, L, and S taken from the NIST ASD. This means that for the levels presented here, the LS-coupling holds with good precision. The only experimental value of the g factor listed in the NIST ASD was measured by David et al. [36] for the $5s5p^2\,^4P_{3/2}$ level to be equal to 2.6609(7) and is in good agreement with our result.

We give oscillator strengths of selected E1 transitions in Table 2. The reported values are calculated in the

length gauge. We checked that for strong transitions the agreement between the length and velocity gauges is good (for weaker transitions the agreement is a bit worse).

We compared our results with the most recent MCDHF calculations of Atalay et al. [31], the Breit–Pauli CI calculations of Oliver and Hubbert [27], as well as the all-order relativistic many-body perturbation theory calculations of Safronova et al. [26]. In the work of Safronova et al. [26], Sn II was considered as a one-electron system with the $5s^2$ shell belonging to the core, so the CI part of the present method was not included in the calculations. The results of all calculations based on varied approaches are in good agreement. The only noticeable difference is for the $5s^25p\,^2P^o_{3/2} - 5s^27s\,^2S_{1/2}$ transition, where the f-value of Safronova et al. [26] is significantly smaller compared to the results of other calculations. Given the good agreement for electric dipole transitions, we now turn to magnetic dipole and electric quadrupole transitions.

Tables 3 and 4 show, respectively, our results for the M1 and E2 transitions between the calculated levels. We do not list transitions with wavelengths larger than $4\,\mu m$ and M1 reduced matrix elements smaller than $0.01\mu_B$, where μ_B is the Bohr magneton. In Table 3,

Table 2 Oscillator strengths f of electric dipole (E1) transitions in Sn II

Transition	λ^{calc} (Å)	This work	Atalay et al. [31]	Oliver and Hubbert [27][a]	Safronova et al. [26]
$5s^25p\ ^2P^o_{1/2} - 5s^26d\ ^2D_{3/2}$	1109	1.70E−1	1.608E−1	1.722E−1	
$5s^25p\ ^2P^o_{3/2} - 5s^26d\ ^2D_{5/2}$	1161	1.64E−1	1.545E−1	1.665E−1	
$5s^25p\ ^2P^o_{3/2} - 5s^26d\ ^2D_{3/2}$	1163	2.65E−2	2.568E−2	2.591E−2	
$5s^25p\ ^2P^o_{3/2} - 5s^27s\ ^2S_{1/2}$	1220	3.91E−2	3.92E−2	3.737E−2	1.50E−2
$5s^25p\ ^2P^o_{1/2} - 5s^25d\ ^2D_{3/2}$	1398	1.25E+0	1.240E+0	1.205E+0	
$5s^25p\ ^2P^o_{3/2} - 5s^25d\ ^2D_{5/2}$	1472	9.84E−1	9.793E−1	9.524E−1	
$5s^25p\ ^2P^o_{3/2} - 5s^25d\ ^2D_{3/2}$	1487	5.12E−2	4.998E−2	5.275E−2	
$5s^25p\ ^2P^o_{1/2} - 5s5p^2\ ^2D_{3/2}$	1688	1.31E−2	1.194E−2	2.585E−2	
$5s^25p\ ^2P^o_{1/2} - 5s^26s\ ^2S_{1/2}$	1758	1.39E−1	1.371E−1	1.409E−1	1.47E−1
$5s^25p\ ^2P^o_{3/2} - 5s5p^2\ ^2D_{5/2}$	1796	3.55E−2	3.280E−2	4.738E−2	
$5s^25p\ ^2P^o_{3/2} - 5s5p^2\ ^2D_{3/2}$	1818	9.51E−3	0.916E−2	1.112E−2	
$5s^25p\ ^2P^o_{3/2} - 5s^26s\ ^2S_{1/2}$	1900	1.47E−1	1.459E−2	1.502E−1	1.56E−1
$5s^26p\ ^2P^o_{1/2} - 5s^28s\ ^2S_{1/2}$	3683	3.84E−2			3.00E−2
$5s^26p\ ^2P^o_{3/2} - 5s^28s\ ^2S_{1/2}$	3807	3.80E−2			2.94E−2
$5s^25d\ ^2D_{3/2} - 5s^27p\ ^2P^o_{3/2}$	4821	1.26E−3	1.317E−3	1.393E−3	
$5s^25d\ ^2D_{3/2} - 5s^27p\ ^2P^o_{1/2}$	4910	9.46E−3	9.505E−3	9.953E−3	
$5s^25d\ ^2D_{5/2} - 5s^27p\ ^2P^o_{3/2}$	4981	1.04E−2	1.083E−2	1.196E−2	
$5s^26p\ ^2P^o_{1/2} - 5s^26d\ ^2D_{3/2}$	5333	8.52E−1	8.410E−1	8.412E−1	
$5s^26p\ ^2P^o_{3/2} - 5s^26d\ ^2D_{5/2}$	5547	8.12E−1	7.978E−1	7.884E−1	
$5s^26p\ ^2P^o_{3/2} - 5s^26d\ ^2D_{3/2}$	5596	9.15E−2	9.040E−2	8.978E−2	
$5s^25d\ ^2D_{3/2} - 5s^24f\ ^2F^o_{5/2}$	5649	5.31E−1	5.590E−1	5.449E−1	
$5s^25d\ ^2D_{5/2} - 5s^24f\ ^2F^o_{5/2}$	5870	2.47E−2	2.622E−2	2.591E−2	
$5s^25d\ ^2D_{5/2} - 5s^24f\ ^2F^o_{7/2}$	5872	4.94E−1	5.250E−1	5.17E−1	
$5s^26s\ ^2S_{1/2} - 5s^26p\ ^2P^o_{3/2}$	6473	8.70E−1	9.115E−1	8.783E−1	8.63E−1
$5s^26p\ ^2P^o_{1/2} - 5s^27s\ ^2S_{1/2}$	6768	2.61E−1	2.599E−1	2.620E−1	2.65E−1
$5s^26s\ ^2S_{1/2} - 5s^26p\ ^2P^o_{1/2}$	6865	4.17E−1	4.382E−1	4.207E−1	4.14E−1
$5s^26p\ ^2P^o_{3/2} - 5s^27s\ ^2S_{1/2}$	7198	2.82E−1	2.808E−1	2.808E−1	2.86E−1
$5s5p^2\ ^2D_{3/2} - 5s^26p\ ^2P^o_{3/2}$	7640	1.69E−2	1.754E−2	1.859E−2	
$5s5p^2\ ^2D_{5/2} - 5s^26p\ ^2P^o_{3/2}$	8065	1.04E−1	1.087E−1	1.133E−1	
$5s5p^2\ ^2D_{3/2} - 5s^26p\ ^2P^o_{1/2}$	8192	8.32E−2	8.728E−2	9.166E−2	
$5s^27p\ ^2P^o_{1/2} - 5s^28s\ ^2S_{1/2}$	14867	3.57E−1			3.79E−1
$5s^27p\ ^2P^o_{3/2} - 5s^28s\ ^2S_{1/2}$	15748	3.76E−1			4.06E−1
$5s^27s\ ^2S_{1/2} - 5s^27p\ ^2P^o_{3/2}$	16600	1.21E+0	1.234E+0	1.225E+0	1.18E+0
$5s^27s\ ^2S_{1/2} - 5s^27p\ ^2P^o_{1/2}$	17706	5.82E−1	5.980E−1	5.897E−1	5.71E−1

[a] The fine-tuned calculation in the length gauge

there are only seven transitions between odd levels; all other transitions are between even levels.

The M1 and E2 transitions between the $5s^25p\ ^2P^o_{3/2} - 5s^25p\ ^2P^o_{1/2}$ levels of the ground term have previously been calculated by Garstang [37], Warner [38], and Biémont et al. [39]. The comparison of the present results with their predicted values is given in Table 5.

One finds that this line is dominated by the M1 transition, and all theoretical predictions are in good agreement. We would like to stress that our approach is *ab initio* and does not use experimental parameters such as the observed energies of the levels as input, ensuring that accurate results can be obtained even in cases where no experimental energy values are available.

4 Astrophysical application

As a demonstration of how these types of data are useful for astrophysical studies, we present an exploration of the presence of forbidden Sn II transitions in the observations of the kilonova, AT2017gfo. Analysis of the light curves and spectra of AT2017gfo provide evidence for $\sim 0.01-0.05\,\mathrm{M_\odot}$ of r-process material being ejected at speeds $\gtrsim 0.1\,c$ (see, e.g., [5, 40–44]). This material rapidly expanded and cooled, leading to observed spectra appearing to be dominated by emission features after ~ 1 week. At these phases, Gillanders et al. [14] propose that the observed features can be interpreted as emission arising from a quasi-nebular regime. If this is indeed the case, then we can reasonably expect these features to be produced by forbidden transitions, as is routinely observed for late-time nebular phase supernova spectra (see, e.g., [45]). For the

Table 3 Magnetic dipole (M1) transition probabilities in Sn II together with the calculated energy differences and wavelengths

Upper level	Lower level	ΔE^{calc} (cm^{-1})	λ^{calc} (Å)	A^{M1} (s^{-1})
$5s^27p\ ^2P^o_{3/2}$	$5s^25p\ ^2P^o_{1/2}$	92259	1084	1.35E+0
$5s^27p\ ^2P^o_{1/2}$	$5s^25p\ ^2P^o_{3/2}$	87630	1141	2.73E+0
$5s^26p\ ^2P^o_{3/2}$	$5s^25p\ ^2P^o_{1/2}$	72343	1382	2.49E+0
$5s^26p\ ^2P^o_{1/2}$	$5s^25p\ ^2P^o_{3/2}$	67207	1488	4.53E+0
$5s^26d\ ^2D_{3/2}$	$5s5p^2\ ^4P_{3/2}$	41253	2424	5.06E−2
$5s^26d\ ^2D_{5/2}$	$5s5p^2\ ^4P_{5/2}$	39048	2561	1.08E−1
$5s^27s\ ^2S_{1/2}$	$5s5p^2\ ^4P_{3/2}$	37275	2683	2.03E−1
$5s5p^2\ ^2P_{3/2}$	$5s5p^2\ ^4P_{1/2}$	34572	2893	2.35E−1
$5s5p^2\ ^2P_{1/2}$	$5s5p^2\ ^4P_{1/2}$	33520	2983	1.14E−1
$5s5p^2\ ^2P_{3/2}$	$5s5p^2\ ^4P_{3/2}$	32646	3063	9.62E−1
$5s5p^2\ ^2P_{1/2}$	$5s5p^2\ ^4P_{3/2}$	31594	3165	6.70E+0
$5s5p^2\ ^2P_{3/2}$	$5s5p^2\ ^4P_{5/2}$	30284	3302	1.86E−1
$5s5p^2\ ^2S_{1/2}$	$5s5p^2\ ^4P_{1/2}$	29036	3444	3.96E+0
$5s5p^2\ ^2S_{1/2}$	$5s5p^2\ ^4P_{3/2}$	27110	3689	6.45E+0
$5s5p^2\ ^2P_{3/2}$	$5s^26s\ ^2S_{1/2}$	24713	4047	1.08E−2
$5s^25d\ ^2D_{3/2}$	$5s5p^2\ ^4P_{1/2}$	24481	4085	1.34E−1
$5s5p^2\ ^2P_{1/2}$	$5s^26s\ ^2S_{1/2}$	23661	4226	1.99E−2
$5s^25d\ ^2D_{5/2}$	$5s5p^2\ ^4P_{3/2}$	23221	4306	4.81E−1
$5s^25d\ ^2D_{3/2}$	$5s5p^2\ ^4P_{3/2}$	22555	4434	4.12E−1
$5s^28s\ ^2S_{1/2}$	$5s5p^2\ ^2S_{1/2}$	22538	4437	1.83E−2
$5s5p^2\ ^2P_{3/2}$	$5s5p^2\ ^2D_{3/2}$	22354	4474	1.16E+0
$5s5p^2\ ^2P_{3/2}$	$5s5p^2\ ^2D_{5/2}$	21663	4616	6.78E−1
$5s5p^2\ ^2P_{1/2}$	$5s5p^2\ ^2D_{3/2}$	21302	4694	4.51E−1
$5s^25d\ ^2D_{5/2}$	$5s5p^2\ ^4P_{5/2}$	20859	4794	1.55E+0
$5s^27p\ ^2P^o_{3/2}$	$5s^26p\ ^2P^o_{1/2}$	20799	4808	6.52E−2
$5s^25d\ ^2D_{3/2}$	$5s5p^2\ ^4P_{5/2}$	20194	4952	2.10E−1
$5s^27p\ ^2P^o_{1/2}$	$5s^26p\ ^2P^o_{3/2}$	19541	5118	1.16E−1
$5s5p^2\ ^2S_{1/2}$	$5s^26s\ ^2S_{1/2}$	19178	5214	1.17E−2
$5s^26d\ ^2D_{5/2}$	$5s^25d\ ^2D_{3/2}$	18855	5304	1.23E−2
$5s^28s\ ^2S_{1/2}$	$5s5p^2\ ^2P_{1/2}$	18055	5539	1.70E−2
$5s^26d\ ^2D_{3/2}$	$5s^25d\ ^2D_{5/2}$	18032	5546	6.63E−3
$5s5p^2\ ^2S_{1/2}$	$5s5p^2\ ^2D_{3/2}$	16818	5946	1.18E−1
$5s^26d\ ^2D_{3/2}$	$5s5p^2\ ^2S_{1/2}$	14142	7071	1.47E−2
$5s^25d\ ^2D_{5/2}$	$5s5p^2\ ^2D_{3/2}$	12929	7735	1.33E−2
$5s^28s\ ^2S_{1/2}$	$5s^27s\ ^2S_{1/2}$	12374	8082	3.13E−1
$5s^25d\ ^2D_{3/2}$	$5s5p^2\ ^2D_{3/2}$	12263	8154	6.16E−3
$5s^25d\ ^2D_{5/2}$	$5s5p^2\ ^2D_{5/2}$	12239	8171	1.14E−2
$5s5p^2\ ^2D_{3/2}$	$5s5p^2\ ^4P_{1/2}$	12218	8185	1.30E−1
$5s^25d\ ^2D_{3/2}$	$5s5p^2\ ^2D_{5/2}$	11573	8641	3.51E−2
$5s5p^2\ ^2D_{5/2}$	$5s5p^2\ ^4P_{3/2}$	10982	9106	4.07E−1
$5s5p^2\ ^2D_{3/2}$	$5s5p^2\ ^4P_{3/2}$	10292	9716	3.09E−1
$5s^27s\ ^2S_{1/2}$	$5s5p^2\ ^2S_{1/2}$	10164	9838	4.64E−2
$5s5p^2\ ^2P_{3/2}$	$5s^25d\ ^2D_{3/2}$	10090	9910	5.16E−1
$5s^26d\ ^2D_{3/2}$	$5s5p^2\ ^2P_{1/2}$	9659	10353	4.56E−3
$5s5p^2\ ^2P_{3/2}$	$5s^25d\ ^2D_{5/2}$	9425	10610	2.62E−1
$5s5p^2\ ^2P_{1/2}$	$5s^25d\ ^2D_{3/2}$	9038	11064	1.27E−1
$5s^26d\ ^2D_{5/2}$	$5s5p^2\ ^2P_{3/2}$	8764	11410	7.50E−3
$5s5p^2\ ^2D_{5/2}$	$5s5p^2\ ^4P_{5/2}$	8621	11600	7.91E−1
$5s^26d\ ^2D_{3/2}$	$5s5p^2\ ^2P_{3/2}$	8607	11619	2.05E−2
$5s^28s\ ^2S_{1/2}$	$5s^26d\ ^2D_{3/2}$	8396	11911	3.56E−2
$5s5p^2\ ^2D_{3/2}$	$5s5p^2\ ^4P_{5/2}$	7930	12610	1.13E−1
$5s^27s\ ^2S_{1/2}$	$5s5p^2\ ^2P_{1/2}$	5681	17603	7.79E−3
$5s5p^2\ ^2P_{3/2}$	$5s5p^2\ ^2S_{1/2}$	5535	18066	7.45E−1
$5s^27s\ ^2S_{1/2}$	$5s5p^2\ ^2P_{3/2}$	4629	21604	4.16E−3

Table 3 continued

Upper level	Lower level	ΔE^{calc} (cm^{-1})	λ^{calc} (Å)	A^{M1} (s^{-1})
$5s5p^2\ ^2S_{1/2}$	$5s^25d\ ^2D_{3/2}$	4555	21954	1.46E$-$2
$5s5p^2\ ^2P_{1/2}$	$5s5p^2\ ^2S_{1/2}$	4483	22304	8.12E$-$1
$5s^25p\ ^2P^o_{3/2}$	$5s^25p\ ^2P^o_{1/2}$	4253	23512	6.90E$-$1

following analysis, we undertake the same method out-lined by Gillanders et al. [14] for their study of late-time Pt and Au emission. The main steps of the analysis are briefly summarized below, but we refer the reader to Ref. [14] for details.

The high ejecta velocity and low ejecta mass ($v \simeq 0.2\,c$, $M \simeq 0.03\,\mathrm{M_\odot}$; Ref. [5]) of AT2017gfo result in an electron density, $n_e \lesssim 10^9\,\mathrm{cm^{-3}}$ after $\gtrsim 3$ days (assuming a uniformly expanding sphere, composed of singly ionized ejecta and a filling factor of 0.1; see Ref. [45]). In this regime, transitions with Einstein A-coefficients $\ll 100\,\mathrm{s^{-1}}$ are needed to favor radiative de-excitation [45]. Transitions that meet this criterion may produce detectable nebular emission features in the spectra of AT2017gfo.

We expect the effects of strong permitted transitions to be negligible at late times, since they will have significantly depopulated upper levels (relative to local thermal equilibrium; LTE). Therefore, we discard all transitions that originate from an upper level that is not *metastable*. Ref. [14] defines a metastable level as any level that has a mean radiative lifetime, $\tau_{\mathrm{rad}} \geq 10^{-2}\,\mathrm{s}$, where τ_{rad} is the inverse of the sum of the A-values of all transitions that originate from that level. For the remaining transitions, we assume LTE level populations (as in Ref. [14]).[1]

Next, we need an estimate for the mass of Sn II in the ejecta of AT2017gfo. Gillanders et al. [15] present realistic composition profiles for KN ejecta, and their favored composition for the ejecta of AT2017gfo (for +2.4 days onward) contains ~ 20 per cent (by mass) of Sn. Using the Saha ionization equation we determine that, for temperatures $\gtrsim 3000\,\mathrm{K}$ and electron densities $\sim 10^8\,\mathrm{cm^{-3}}$, almost all of the Sn in the ejecta is expected to be singly ionized. Combining this with the ejecta masses invoked for AT2017gfo, we propose that Sn II masses on the order $\sim$ a few $10^{-3}\,\mathrm{M_\odot}$ can be reasonably expected, and so we invoke $M_{\mathrm{Sn\,II}} = 10^{-3}\,\mathrm{M_\odot}$ for our analysis here.

Pairing this mass estimate with our estimated level populations, we can directly calculate the luminosity emitted by each transition (L_{em}), using:

$$L_{\mathrm{em}} = A_{ul}\, N_u \left(\frac{hc}{\lambda} \right), \qquad (5)$$

where A_{ul} is the A-value for the de-excitation transition between some upper level u and lower level l, N_u is the number of atoms/ions in the excited state, and λ is the wavelength of the transition. To visualize the strengths of the lines relative to the observed features of AT2017gfo, we generate simple synthetic emission spectra (as in Ref. [14]). To do this, we first generate Gaussian emission features for each transition, with full-width, half-maximum (FWHM) velocities of $0.1\,c$, and peak values determined from our L_{em} values (see Ref. [14]). These individual Gaussians were then co-added to form a single composite emission spectrum, which illustrates the absolute luminosity expected for Sn II transitions in kilonova ejecta. Note that we generate synthetic emission spectra for each transition type (i.e., E1, M1, E2) separately.

From this approach, we can investigate whether any Sn II transitions are expected to be prominent/detectable for typical KN ejecta conditions. We can also investigate how the strength of the features vary as we alter our ejecta temperature across some range of plausible values for kilonova ejecta at late times ($T \in [2500, 3500, 4500]\,\mathrm{K}$). With these simple emission spectra, we compare to the observed spectra of AT2017gfo and determine whether any prominent features are coincident with the emission features in the observed data.

For all model temperatures explored, we expect to see a prominent feature centered at $\lambda = 23512$ Å, which is produced by both an M1 and an E2 transition. This is the strongest feature across all model temperatures and indeed is the only line that we predict is prominent/detectable (for our assumed ejecta properties). Specifically, in our 4500 K model, we compute an emitted line luminosity of $\sim 2.0 \times 10^{39}\,\mathrm{erg\,s^{-1}}$, which is comparable to observed feature strengths in the late-time spectra of AT2017gfo [14]. For our lowest temperature model (2500 K), we compute an emitted line luminosity of $\sim 8.5 \times 10^{38}\,\mathrm{erg\,s^{-1}}$ for this transition (which should still be luminous enough to be detectable). As such, we expect this feature to be observable in kilonova events that synthesize significant amounts of Sn (provided they exhibit ejecta properties similar to those assumed here).

In Fig. 1, we present comparisons between the E1, M1 and E2 synthetic emission spectra for Sn II and the late-time spectra of AT2017gfo (taken from Refs. [4,5]). We find that E1 transitions produce no observable features, as these have been disfavored by the radiative lifetime cut. We see that the M1 23512 Å feature is comparably as strong as some of the emission features present in the

---

[1] This approximation possibly introduces some uncertainty into our level populations, although metastable, low-lying levels (which we are most sensitive to in our present study) are the levels expected to most closely match LTE.

Table 4 Probabilities of electric quadrupole (E2) transitions in Sn II together with the calculated energy differences and wavelengths

Upper level	Lower level	ΔE^{calc} (cm^{-1})	λ^{calc} (Å)	A^{E2} (s^{-1})
$5s^2 7p\ ^2P^o_{3/2}$	$5s^2 5p\ ^2P^o_{1/2}$	92259	1084	9.02E+2
$5s^2 4f\ ^2F^o_{5/2}$	$5s^2 5p\ ^2P^o_{1/2}$	89218	1121	7.48E+3
$5s^2 7p\ ^2P^o_{3/2}$	$5s^2 5p\ ^2P^o_{3/2}$	88006	1136	7.92E+2
$5s^2 7p\ ^2P^o_{1/2}$	$5s^2 5p\ ^2P^o_{3/2}$	87630	1141	1.64E+3
$5s^2 4f\ ^2F^o_{7/2}$	$5s^2 5p\ ^2P^o_{3/2}$	84960	1177	8.94E+3
$5s^2 4f\ ^2F^o_{5/2}$	$5s^2 5p\ ^2P^o_{3/2}$	84965	1177	1.98E+3
$5s^2 6p\ ^2P^o_{3/2}$	$5s^2 5p\ ^2P^o_{1/2}$	72343	1382	1.48E+3
$5s^2 6p\ ^2P^o_{3/2}$	$5s^2 5p\ ^2P^o_{3/2}$	68090	1469	1.39E+3
$5s^2 6p\ ^2P^o_{1/2}$	$5s^2 5p\ ^2P^o_{3/2}$	67207	1488	2.95E+3
$5s^2 8s\ ^2S_{1/2}$	$5s5p^2\ ^4P_{3/2}$	49649	2014	3.23E−3
$5s^2 8s\ ^2S_{1/2}$	$5s5p^2\ ^4P_{5/2}$	47287	2115	1.22E−1
$5s^2 6d\ ^2D_{5/2}$	$5s5p^2\ ^4P_{1/2}$	43336	2308	5.73E−2
$5s^2 6d\ ^2D_{3/2}$	$5s5p^2\ ^4P_{1/2}$	43179	2316	4.94E−2
$5s^2 6d\ ^2D_{5/2}$	$5s5p^2\ ^4P_{3/2}$	41410	2415	4.50E−2
$5s^2 6d\ ^2D_{3/2}$	$5s5p^2\ ^4P_{3/2}$	41253	2424	1.33E−1
$5s^2 8s\ ^2S_{1/2}$	$5s5p^2\ ^2D_{3/2}$	39356	2541	1.50E+1
$5s^2 6d\ ^2D_{5/2}$	$5s5p^2\ ^4P_{5/2}$	39048	2561	1.63E+0
$5s^2 6d\ ^2D_{3/2}$	$5s5p^2\ ^4P_{5/2}$	38891	2571	6.30E−1
$5s^2 8s\ ^2S_{1/2}$	$5s5p^2\ ^2D_{5/2}$	38666	2586	2.52E+1
$5s^2 7s\ ^2S_{1/2}$	$5s5p^2\ ^4P_{3/2}$	37275	2683	4.26E−2
$5s^2 7s\ ^2S_{1/2}$	$5s5p^2\ ^4P_{5/2}$	34913	2864	6.82E−1
$5s5p^2\ ^2P_{3/2}$	$5s5p^2\ ^4P_{1/2}$	34572	2893	4.64E−2
$5s^2 6d\ ^2D_{5/2}$	$5s^2 6s\ ^2S_{1/2}$	33477	2987	5.06E+2
$5s^2 6d\ ^2D_{3/2}$	$5s^2 6s\ ^2S_{1/2}$	33320	3001	5.09E+2
$5s5p^2\ ^2P_{3/2}$	$5s5p^2\ ^4P_{3/2}$	32646	3063	1.53E−1
$5s5p^2\ ^2P_{1/2}$	$5s5p^2\ ^4P_{3/2}$	31594	3165	2.35E−1
$5s^2 6d\ ^2D_{5/2}$	$5s5p^2\ ^2D_{3/2}$	31118	3214	1.38E+1
$5s^2 6d\ ^2D_{3/2}$	$5s5p^2\ ^2D_{3/2}$	30961	3230	4.85E+1
$5s^2 6d\ ^2D_{5/2}$	$5s5p^2\ ^2D_{5/2}$	30428	3287	5.52E+1
$5s5p^2\ ^2P_{3/2}$	$5s5p^2\ ^4P_{5/2}$	30284	3302	8.82E−2
$5s^2 6d\ ^2D_{3/2}$	$5s5p^2\ ^2D_{5/2}$	30270	3304	2.11E+1
$5s5p^2\ ^2P_{1/2}$	$5s5p^2\ ^4P_{5/2}$	29232	3421	8.64E−1
$5s5p^2\ ^2S_{1/2}$	$5s5p^2\ ^4P_{3/2}$	27110	3689	6.63E−3
$5s^2 8s\ ^2S_{1/2}$	$5s^2 5d\ ^2D_{3/2}$	27093	3691	8.40E+0
$5s^2 7s\ ^2S_{1/2}$	$5s5p^2\ ^2D_{3/2}$	26983	3706	3.05E+1
$5s^2 8s\ ^2S_{1/2}$	$5s^2 5d\ ^2D_{5/2}$	26428	3784	1.05E+1
$5s^2 7s\ ^2S_{1/2}$	$5s5p^2\ ^2D_{5/2}$	26292	3803	4.74E+1
$5s^2 5d\ ^2D_{5/2}$	$5s5p^2\ ^4P_{1/2}$	25147	3977	2.45E−2
$5s5p^2\ ^2S_{1/2}$	$5s5p^2\ ^4P_{5/2}$	24749	4041	1.89E−1
$5s5p^2\ ^2P_{3/2}$	$5s^2 6s\ ^2S_{1/2}$	24713	4047	2.17E+0
$5s^2 5d\ ^2D_{3/2}$	$5s5p^2\ ^4P_{1/2}$	24481	4085	8.96E−2
$5s^2 5d\ ^2D_{5/2}$	$5s5p^2\ ^4P_{3/2}$	23221	4306	4.12E−2
$5s^2 5d\ ^2D_{3/2}$	$5s5p^2\ ^4P_{3/2}$	22555	4434	1.21E−3
$5s5p^2\ ^2P_{3/2}$	$5s5p^2\ ^2D_{3/2}$	22354	4474	4.92E−3
$5s5p^2\ ^2P_{3/2}$	$5s5p^2\ ^2D_{5/2}$	21663	4616	1.87E−3
$5s5p^2\ ^2P_{1/2}$	$5s5p^2\ ^2D_{3/2}$	21302	4694	2.60E+0
$5s^2 5d\ ^2D_{5/2}$	$5s5p^2\ ^4P_{5/2}$	20859	4794	3.44E−2
$5s^2 7p\ ^2P^o_{3/2}$	$5s^2 6p\ ^2P^o_{1/2}$	20799	4808	7.56E+1
$5s5p^2\ ^2P_{1/2}$	$5s5p^2\ ^2D_{5/2}$	20612	4852	4.71E+0
$5s^2 5d\ ^2D_{3/2}$	$5s5p^2\ ^4P_{5/2}$	20194	4952	4.81E−3
$5s^2 7p\ ^2P^o_{3/2}$	$5s^2 6p\ ^2P^o_{3/2}$	19917	5021	7.39E+1
$5s^2 7p\ ^2P^o_{1/2}$	$5s^2 6p\ ^2P^o_{3/2}$	19541	5118	1.51E+2
$5s^2 6d\ ^2D_{5/2}$	$5s^2 5d\ ^2D_{3/2}$	18855	5304	7.18E+0
$5s^2 6d\ ^2D_{3/2}$	$5s^2 5d\ ^2D_{3/2}$	18697	5348	2.47E+1

Table 4 continued

Upper level	Lower level	ΔE^{calc} (cm^{-1})	λ^{calc} (Å)	A^{E2} (s^{-1})
$5s^26d\ ^2D_{5/2}$	$5s^25d\ ^2D_{5/2}$	18189	5498	2.65E+1
$5s^26d\ ^2D_{3/2}$	$5s^25d\ ^2D_{5/2}$	18032	5546	9.73E+0
$5s^24f\ ^2F^o_{5/2}$	$5s^26p\ ^2P^o_{1/2}$	17758	5631	1.36E+2
$5s^28s\ ^2S_{1/2}$	$5s5p^2\ ^2P_{3/2}$	17003	5881	2.70E−2
$5s^24f\ ^2F^o_{5/2}$	$5s^26p\ ^2P^o_{3/2}$	16876	5926	3.20E+1
$5s^24f\ ^2F^o_{7/2}$	$5s^26p\ ^2P^o_{3/2}$	16870	5928	1.44E+2
$5s5p^2\ ^2S_{1/2}$	$5s5p^2\ ^2D_{3/2}$	16818	5946	2.03E+0
$5s5p^2\ ^2S_{1/2}$	$5s5p^2\ ^2D_{5/2}$	16128	6200	1.65E+0
$5s^25d\ ^2D_{5/2}$	$5s^26s\ ^2S_{1/2}$	15288	6541	1.29E+1
$5s^27s\ ^2S_{1/2}$	$5s^25d\ ^2D_{3/2}$	14719	6794	1.34E+1
$5s^25d\ ^2D_{3/2}$	$5s^26s\ ^2S_{1/2}$	14623	6839	1.03E+1
$5s^26d\ ^2D_{5/2}$	$5s5p^2\ ^2S_{1/2}$	14300	6993	7.18E−2
$5s^26d\ ^2D_{3/2}$	$5s5p^2\ ^2S_{1/2}$	14142	7071	8.92E−2
$5s^27s\ ^2S_{1/2}$	$5s^25d\ ^2D_{5/2}$	14054	7116	1.75E+1
$5s^25d\ ^2D_{5/2}$	$5s5p^2\ ^2D_{3/2}$	12929	7735	1.37E−1
$5s5p^2\ ^2D_{5/2}$	$5s5p^2\ ^4P_{1/2}$	12908	7747	1.62E−3
$5s^25d\ ^2D_{3/2}$	$5s5p^2\ ^2D_{3/2}$	12263	8154	4.00E−1
$5s^25d\ ^2D_{5/2}$	$5s5p^2\ ^2D_{5/2}$	12239	8171	5.18E−1
$5s5p^2\ ^2D_{3/2}$	$5s5p^2\ ^4P_{1/2}$	12218	8185	2.84E−3
$5s^25d\ ^2D_{3/2}$	$5s5p^2\ ^2D_{5/2}$	11573	8641	1.59E−1
$5s5p^2\ ^2D_{5/2}$	$5s5p^2\ ^4P_{3/2}$	10982	9106	1.33E−2
$5s5p^2\ ^2D_{3/2}$	$5s5p^2\ ^4P_{3/2}$	10292	9716	8.21E−4
$5s5p^2\ ^2P_{3/2}$	$5s^25d\ ^2D_{3/2}$	10090	9910	5.80E−2
$5s^26d\ ^2D_{5/2}$	$5s5p^2\ ^2P_{1/2}$	9816	10187	2.04E−1
$5s^26d\ ^2D_{3/2}$	$5s5p^2\ ^2P_{1/2}$	9659	10353	1.76E−1
$5s5p^2\ ^2P_{3/2}$	$5s^25d\ ^2D_{5/2}$	9425	10610	8.92E−3
$5s5p^2\ ^2P_{1/2}$	$5s^25d\ ^2D_{3/2}$	9038	11064	1.41E−1
$5s^26d\ ^2D_{5/2}$	$5s5p^2\ ^2P_{3/2}$	8764	11410	1.29E−2
$5s5p^2\ ^2D_{5/2}$	$5s5p^2\ ^4P_{5/2}$	8621	11600	1.95E−2
$5s^26d\ ^2D_{3/2}$	$5s5p^2\ ^2P_{3/2}$	8607	11619	3.94E−2
$5s^28s\ ^2S_{1/2}$	$5s^26d\ ^2D_{3/2}$	8396	11911	8.89E+0
$5s5p^2\ ^2P_{1/2}$	$5s^25d\ ^2D_{5/2}$	8373	11943	1.96E−1
$5s^28s\ ^2S_{1/2}$	$5s^26d\ ^2D_{5/2}$	8238	12138	1.10E+1
$5s^26s\ ^2S_{1/2}$	$5s5p^2\ ^4P_{3/2}$	7933	12606	3.77E−4
$5s5p^2\ ^2D_{3/2}$	$5s5p^2\ ^4P_{5/2}$	7930	12610	4.30E−3
$5s^26s\ ^2S_{1/2}$	$5s5p^2\ ^4P_{5/2}$	5571	17950	1.29E−3
$5s5p^2\ ^2P_{3/2}$	$5s5p^2\ ^2S_{1/2}$	5535	18066	2.74E−3
$5s^27s\ ^2S_{1/2}$	$5s5p^2\ ^2P_{3/2}$	4629	21604	2.80E−3
$5s5p^2\ ^2S_{1/2}$	$5s^25d\ ^2D_{3/2}$	4555	21954	4.49E−3
$5s5p^2\ ^4P_{5/2}$	$5s5p^2\ ^4P_{1/2}$	4288	23322	1.69E−3
$5s^25p\ ^2P^o_{3/2}$	$5s^25p\ ^2P^o_{1/2}$	4253	23512	2.59E−3
$5s^26d\ ^2D_{5/2}$	$5s^27s\ ^2S_{1/2}$	4135	24181	3.92E−1
$5s^26d\ ^2D_{3/2}$	$5s^27s\ ^2S_{1/2}$	3978	25139	3.25E−1
$5s5p^2\ ^2S_{1/2}$	$5s^25d\ ^2D_{5/2}$	3889	25711	2.56E−3
$5s5p^2\ ^2D_{5/2}$	$5s^26s\ ^2S_{1/2}$	3049	32793	2.10E−3
$5s^27p\ ^2P^o_{3/2}$	$5s^24f\ ^2F^o_{7/2}$	3047	32823	7.81E−2
$5s^27p\ ^2P^o_{3/2}$	$5s^24f\ ^2F^o_{5/2}$	3041	32881	1.30E−2
$5s^27p\ ^2P^o_{1/2}$	$5s^24f\ ^2F^o_{5/2}$	2665	37523	4.90E−2

observed data,[2] although it is too red to be responsible for the observed feature in AT2017gfo at $\sim 2.1\,\mu$m. Aside from this feature, we do not see any other promi-nent emission features in the wavelength range of the AT2017gfo spectra.

The [Sn II] transition at $\lambda = 23512\,$Å is expected to be the *only* detectable Sn II line produced by late-time kilonova ejecta, across a range of plausible ejecta temperatures. A modest mass of Sn II ($M_{\mathrm{Sn\,II}} = 10^{-3}\,\mathrm{M}_\odot$) is sufficient to produce a line strength on par with the emission features observed in the late-time spectra of

---

[2] The equivalent E2 transition produces no observable feature in Fig. 1, since its *A*-value is significantly smaller than the M1 transition ($A^{\mathrm{M1}} = 0.69\,\mathrm{s}^{-1}$, versus $A^{\mathrm{E2}} = 0.00259\,\mathrm{s}^{-1}$).

Table 5 Comparison of the M1 and E2 rates A (in s^{-1}) for the $5s^2 5p\ ^2P^o_{3/2} - 5s^2 5p\ ^2P^o_{1/2}$ transition in Sn II

Type	This work	Biémont et al. [39]	Warner [38]	Garstang [37]
M1	6.90E−1	6.940E−1	6.91E−1	6.8E−1
E2	2.59E−3	2.893E−3	2.15E−3	3.5E−3
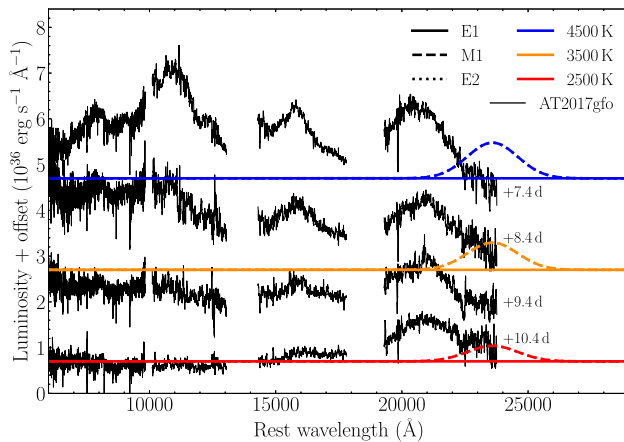
Fig. 1 Sn II E1, M1 and E2 synthetic emission spectra compared with the observed late-time (+7.4−10.4 day) emission spectra of AT2017gfo. Both the observed and synthetic spectra have been offset for clarity. The synthetic spectra presented span a range of temperatures ($T \in$ [2500, 3500, 4500] K), and are plotted as red, orange and blue curves, respectively. The Sn II E1, M1 and E2 emission spectra are plotted as solid, dashed and dotted lines, respectively. No scaling has been applied to either the observed or synthetic spectra

AT2017gfo. Although this line is too red to be responsible for the observed emission feature at $\sim 2.1\,\mu$m in the AT2017gfo spectra, we propose that it can be used as a probe to infer the presence of Sn II in future kilonova events. Such predictions for the expected locations of prominent emission features are of paramount importance for future analyses of new kilonova events, to better constrain their composition profiles.

5 Conclusions

We used the CI + all-order method for evaluating the low-lying energy levels and probabilities of multipole transitions in Sn II. The calculated spectrum well reproduces the observed energy levels. The obtained oscillator strengths of electric dipole transitions are in good agreement with recent theoretical evaluations by other methods. Our newly computed data for probabilities of magnetic dipole and quadrupole transitions allowed us to analyze the AT2017gfo kilonova by generating synthetic emission spectra and comparing them with the observations. We found that, under the adopted reasonable conditions, the M1 transition between the levels of the ground-state doublet leads to the strong spectral feature. Although this transition does not match any prominent features in the AT2017gfo spectra, it

can nevertheless be used as a probe for future kilonova events.

This work demonstrated that atomic data that are currently unavailable for other r-process elements needed for kilonova modeling can be generated using the present approach. This method has been tested on systems with up to six valence electrons [46], so data for elements with a more complicated electronic structure can also be calculated. Alternatively, other methods developed for open d- and f-shell ions [47,48] could be utilized.

Author contributions

All the authors contributed equally to the manuscript.

Data Availability Statement This manuscript has no associated data or the data will not be deposited. [Authors' comment: The datasets generated and analyzed during the current study are available from the corresponding author on reasonable request.]

References

1. E. Biémont, C.J. Zeippen, J. Phys. IV France **01**, 209 (1991)
2. E. Biémont, C.J. Zeippen, Phys. Scr. **1996**, 192 (1996)
3. D.E. Osterbrock, G.J. Ferland, *Astrophysics of gaseous nebulae and active galactic nuclei* 2nd ed (2006)
4. E. Pian, P. D'Avanzo, S. Benetti, M. Branchesi, E. Brocato, S. Campana, E. Cappellaro, S. Covino, V. D'Elia, J.P.U. Fynbo et al., Nature **551**, 67 (2017), arXiv:1710.05858
5. S.J. Smartt, T.W. Chen, A. Jerkstrand, M. Coughlin, E. Kankare, S.A. Sim, M. Fraser, C. Inserra, K. Maguire, K.C. Chambers et al., Nature **551**, 75 (2017). arXiv:1710.05841
6. B.P. Abbott, R. Abbott, T.D. Abbott, F. Acernese, K. Ackley, C. Adams, T. Adams, P. Addesso, R.X. Adhikari, V.B. Adya et al., LIGO scientific collaboration and virgo collaboration. Phys. Rev. Lett. **119**, 161101 (2017)
7. D.M. Siegel, Nat. Rev. Phys. **4**, 306 (2022)
8. E. Pian, Universe **9**, 105 (2023)
9. S. Rosswog, J. Sollerman, U. Feindt, A. Goobar, O. Korobkin, R. Wollaeger, C. Fremling, M.M. Kasliwal, A&A **615**, A132 (2018). arXiv:1710.05445
10. D. Watson, C.J. Hansen, J. Selsing, A. Koch, D.B. Malesani, A.C. Andersen, J.P.U. Fynbo, A. Arcones, A. Bauswein, S. Covino et al., Nature **574**, 497 (2019). arXiv:1910.10510
11. N. Domoto, M. Tanaka, D. Kato, K. Kawaguchi, K. Hotokezaka, S. Wanajo, Astrophys. J. **939**, 8 (2022). arXiv:2206.04232
12. K. Hotokezaka, M. Tanaka, D. Kato, G. Gaigalas, Mon. Not. R. Astron. Soc. **515**, L89 (2022). arXiv:2204.00737
13. M.M. Kasliwal, D. Kasen, R.M. Lau, D.A. Perley, S. Rosswog, E.O. Ofek, K. Hotokezaka, R.R. Chary, J. Sollerman, A. Goobar et al., Mon. Not. R. Astron. Soc. **510**, L7 (2022). arXiv:1812.08708
14. J.H. Gillanders, M. McCann, S.A. Sim, S.J. Smartt, C.P. Ballance, Mon. Not. R. Astron. Soc. **506**, 3560 (2021)
15. J.H. Gillanders, S.J. Smartt, S.A. Sim, A. Bauswein, S. Goriely, Mon. Not. R. Astron. Soc. **515**, 631 (2022)
16. M. Tanaka, D. Kato, G. Gaigalas, K. Kawaguchi, Mon. Not. R. Astron. Soc. **496**, 1369 (2020)
17. L.M. Hobbs, D.E. Welty, D.C. Morton, L. Spitzer, D.G. York, Astrophys. J. **411**, 750 (1993)
18. U.J. Sofia, D.M. Meyer, J.A. Cardelli, Astrophys. J. **522**, L137 (1999)
19. A.R. Foster, G.F. Counsell, H.P. Summers, J. Nucl. Mater. **363**, 152 (2007)
20. T. Andersen, A. Lindgard, J. Phys. B: Atomic Mol. Opt. Phys. **10**, 2359 (1977)
21. R.M. Schectman, S. Cheng, L.J. Curtis, S.R. Federman, M.C. Fritts, R.E. Irving, Astrophys. J. **542**, 400 (2000)
22. G. Duffy, P. van Kampen, P. Dunne, J. Phys. B: Atomic Mol. Opt. Phys. **34**, 3171 (2001)
23. M.A. Lysaght, D. Kilbane, A. Cummings, N. Murphy, P. Dunne, G. O'Sullivan, P. van Kampen, J.T. Costello, E.T. Kennedy, J. Phys. B: Atomic Mol. Opt. Phys. **38**, 4247 (2005)
24. A. Alonso-Medina, C. Colón, Phys. Scr. **61**, 646 (2000)
25. V.A. Dzuba, V.V. Flambaum, Phys. Rev. A **71**, 052509 (2005)
26. U.I. Safronova, M.S. Safronova, M.G. Kozlov, Phys. Rev. A **76**, 022501 (2007)
27. P. Oliver, A. Hibbert, J. Phys. B: Atomic Mol. Opt. Phys. **43**, 074013 (2010)
28. K. Haris, A. Kramida, A. Tauheed, Phys. Scr. **89**, 115403 (2014). arXiv:1312.0261
29. A. Kramida, Y. Ralchenko, J. Reader, and NIST ASD Team, *NIST Atomic Spectra Database*(version 5.10). https://physics.nist.gov/asd [Mon Mar 06 2023]. National Institute of Standards and Technology, Gaithersburg, MD (2022)
30. N. Heidarian, R.E. Irving, S.R. Federman, D.G. Ellis, S. Cheng, L.J. Curtis, J. Phys. B: Atomic Mol. Opt. Phys. **49**, 215002 (2016)
31. B. Atalay, P. Jönsson, T. Brage, J. Quant. Spectrosc. Radiat. Transf. **294**, 108392 (2023)
32. M.S. Safronova, M.G. Kozlov, W.R. Johnson, D. Jiang, Phys. Rev. A **80**, 012516 (2009)
33. V.M. Shabaev, I.I. Tupitsyn, V.A. Yerokhin, Phys. Rev. A **88**, 012513 (2013)
34. I.I. Tupitsyn, M.G. Kozlov, M.S. Safronova, V.M. Shabaev, V.A. Dzuba, Phys. Rev. Lett. **117**, 253001 (2016)
35. M. Kozlov, S. Porsev, M. Safronova, I. Tupitsyn, Comput. Phys. Commun. **195**, 199 (2015)
36. D. David, J. Hamel, J.P. Barrat, Opt. Commun. **32**, 241 (1980)
37. R. Garstang, J. Res. Natl. Bureau Standards Sect. A Phys. Chem. **68**, 61 (1964)
38. B. Warner, ZA **69**, 399 (1968)
39. E. Biémont, J.E. Hansen, P. Quinet, C.J. Zeippen, A&AS **111**, 333 (1995)
40. P.S. Cowperthwaite, E. Berger, V.A. Villar, B.D. Metzger, M. Nicholl, R. Chornock, P.K. Blanchard, W. Fong, R. Margutti, M. Soares-Santos et al., ApJL **848**, L17 (2017). arXiv:1710.05840
41. M.R. Drout, A.L. Piro, B.J. Shappee, C.D. Kilpatrick, J.D. Simon, C. Contreras, D.A. Coulter, R.J. Foley, M.R. Siebert, N. Morrell et al., Science **358**, 1570 (2017). arXiv:1710.05443
42. N.R. Tanvir, A.J. Levan, C. González-Fernández, O. Korobkin, I. Mandel, S. Rosswog, J. Hjorth, P. D'Avanzo, A.S. Fruchter, C.L. Fryer et al., ApJL **848**, L27 (2017). arXiv:1710.05455
43. M.W. Coughlin, T. Dietrich, Z. Doctor, D. Kasen, S. Coughlin, A. Jerkstrand, G. Leloudas, O. McBrien, B.D. Metzger, R. O'Shaughnessy et al., Mon. Not. R. Astron. Soc. **480**, 3871 (2018). arXiv:1805.09371
44. E. Waxman, E.O. Ofek, D. Kushnir, A. Gal-Yam, Mon. Not. R. Astron. Soc. **481**, 3423 (2018). arXiv:1711.09638
45. A. Jerkstrand, in *Handbook of Supernovae*, edited by A.W. Alsabti, P. Murdin (2017), p. 795
46. E.B. Norrgard, D.S. Barker, S.P. Eckel, S.G. Porsev, C. Cheung, M.G. Kozlov, I.I. Tupitsyn, M.S. Safronova, Phys. Rev. A **105** (2022)
47. S. Fritzsche, Atoms **10**, 7 (2022)
48. M.G. Kozlov, I.I. Tupitsyn, A.I. Bondarev, D.V. Mironova, Phys. Rev. A **105**, 052805 (2022)